On the -detection efficiency of a combined Si and plastic stack detector for DESPEC

Nuclear Inst. and Methods in Physics Research, A xxx (xxxx) xxx

Contents lists available at ScienceDirect

Nuclear Inst. and Methods in Physics Research, A

journal homepage: www.elsevier.com/locate/nima

On the β-detection efficiency of a combined Si and plastic stack detector for DESPEC

S. Saha [a,b,*], T. Arici [a], J. Gerl [a], M. Górska [a], N. Pietralla [b], T. Davinson [c], A.I. Morales [d], Zs. Podolyák [e,f]

[a] GSI Helmholtzzentrum für Schwerionenforschung, Planckstraße 1, D-64291 Darmstadt, Germany
[b] Technische Universität Darmstadt, Darmstadt, Germany
[c] University of Edinburgh, School of Physics and Astronomy, Edinburgh EH9 3FD, UK
[d] Instituto de Física Corpuscular, CSIC and Universitat de Valencia, E-46980 Paterna, Spain
[e] Department of Physics, University of Surrey, Guildford, GU2 7XH, UK
[f] ExtreMe Matter Institute EMMI, GSI Helmholtzzentrum für Schwerionenforschung, Planckstraße 1, D-64291 Darmstadt, Germany

ARTICLE INFO

Keywords:
Geant4
β detector
Plastic scintillator
DSSSD

ABSTRACT

A Geant4 simulation has been carried out in order to determine the β-detection efficiency of a rare isotope beam implantation setup, for decay spectroscopy experiments, comprising a number of Double Sided Silicon Strip Detectors (DSSSDs) and two plastic scintillation detectors placed upstream and downstream. The absolute efficiency for the emitted β-particle detection from radioactive fragments implanted in the DSSSDs using fast-timing plastic-scintillator detector, is calculated. The detection efficiency of the setup has been studied with two different distances between the Si layers and plastics. The requirement for the thickness of the Si detector layers and its implication on the β-detection efficiency has been investigated for 1 mm and 300 μm thickness of Si layers. The combined efficiency of DSSSD and plastic detectors were also simulated for two different thicknesses of the DSSSD.

1. Introduction

Plastic scintillator detectors are widely used in nuclear and high energy physics experiments due to their excellent time response, low stopping power, relatively low cost and versatility. These detectors are also commonly used in β decay measurements [1–4] alongside Double Sided Silicon Strip Detectors (DSSSDs) [5]. The fast time response of plastic scintillator detectors and the good position resolution of DSSSD makes them complementary in measurements where high quality of both position and time response are demanded. A closely packed setup comprising stacks of DSSSDs and plastic detectors are chosen for the DEcay SPECtroscopy [6,7] setup, as a part of NUSTAR [8,9] experiments at GSI [10] and FAIR [11,12]. A similar setup was installed previously for decay spectroscopy measurements with radioactive ion beams at RIKEN [13–15]. The DESPEC experiments will use the active implantation detector array, AIDA [16,17] for isomer decay spectroscopy measurements as well as for the spectroscopy of the daughter nucleus post β decay of the implanted fragments. The DESPEC experiments aim at studying extremely rare isotopes produced via fragmentation of heavy nuclei namely ^{238}U [18–20]. The background radioactivity is generally orders of magnitude higher than the rate of decay events from nuclei of interest. As a result, event by event correlation of implantation and decay are necessary to study these implanted isotopes. High stopping power and granularity of the AIDA DSSSD makes it a suitable candidate for an implantation detector [16] whereas plastic detectors provide better timing response. Measurement of the nuclear level lifetime via β-delayed γ spectroscopy provides important information about nuclear deformation, collective properties, and more fundamentally, nucleon–nucleon interactions. The fast timing $LaBr_3$(Ce) detectors are used for the lifetime measurements using γ-γ spectroscopy [21]. For the DESPEC experiments at GSI and FAIR, an array of such LaBr3(Ce) detectors known as Fast Timing Array (FATIMA) [22–25] will be used. To do such studies in β-γ coincidence, one needs very good timing for the beta particle as well. Fast timing β plastic detectors have been planned to be used along with AIDA DSSSD layers to obtain precise time of the β decay for delayed correlation with subsequent γ-rays observed from the excited states of the daughter nucleus in one of the $LaBr_3$(Ce) detectors. Estimation of correlated β-γ yield will be crucial to plan lifetime measurement experiments of very exotic isotopes that can be produced in GSI as part of the FAIR Phase-0 experimental campaign. A detailed simulation of the efficiency and response of the setup after implantation of the radioactive fragments is the key to determine expected detection yield. The present work is performed, in view of a proposed setup, consisting of a stack of three

* Correspondence to: 201-Pinanski, 205 Riverside St, Lowell, MA 01854, USA.
E-mail address: Sudipta_Saha@uml.edu (S. Saha).

https://doi.org/10.1016/j.nima.2020.164196
Received 16 October 2019; Received in revised form 26 May 2020; Accepted 27 May 2020
Available online xxxx
0168-9002/

DSSSDs and two plastic detectors, upstream and downstream of the Si stack for β-γ correlation measurement. The DSSSDs are primarily used for implantation of radioactive fragments and correlation of the subsequent β decay. Information on the position of implanted ions will be obtained from the horizontal(X) and vertical(Y) segmentation of the detectors. The implanted fragments are identified in-flight with standard Bρ-ΔE-Bρ method from the fragment separator [26,27]. The highest efficiency for the detection of ion implantation is achieved when ions are stopped close to the middle of the DSSSD stack. In order to achieve this situation with an arbitrary relativistic beam the particle energy can be tuned to the desired value with a degrader of variable thickness. The subsequent β decay of the fragment after implantation occurs, depending on the β-decay lifetime, a time interval ranging from μs to ms and beyond. The possible long decay time makes direct correlation of the implantation and decay difficult to process electronically. Each implanted fragment and β-particle detected in AIDA DSSSD will be time stamped and have a localized distribution. The identification of the decaying nucleus will be carried out mainly through position correlation of energy deposition of the β particle to the implantation position of the fragment. Lifetime measurement of the excited states of the beta-delayed daughter/grand-daughter of the stated ion-fragments will be carried out via β-γ correlation measurements. Such experiments will require precise time response of the β detector. The proposed plastic detectors could achieve a time resolution of the order of a few hundreds of ps, which is far superior to the time response of the DSSSDs. The design of a setup comprising a stack of DSSSD and plastic detector, requires investigation of the energy loss (E_{loss}) of electrons inside the Si before being absorbed by the plastic. The efficiency of the combined setup, will depend upon the threshold of the detectors (E_{th}), the E_{loss} of the β particles inside the detector material, and the probability of electrons escaping the DSSSD and being detected in the plastic detector. Low energy β particles will have small total E_{loss} in the detector material leading to limited light output in the scintillator. Hence, the actual energy distribution of β-decay probability must be factored into the calculation. This problem has been addressed in this work via Monte-Carlo simulation of the full setup with realistic calculation of the energy distribution of the β decay of a typical fragment of interest. The implanted isotopes decay primarily by β-decay. The required thickness and placement of these detectors for optimal efficiency of the β-decay measurement is investigated in this work. A calculated energy spectrum of β decay of ^{224}At is used as a typical candidate for such a measurement. In addition, the response of the setup with a number of isotopes with known β activity have been investigated. A numerical simulation has been carried out using Geant4 package [28] to find the best possible configuration and thickness of the Si layers. The dependence of the absolute efficiency of the setup on the distance between the DSSSDs and plastic is also investigated. The simulation program developed is a suitably modified version of a previously tested simulation code for modeling the response of a clover-HPGe-detector array [29].

2. Details of simulation framework

2.1. Geometrical model

The simulation geometry consists of three rectangular Si layers (7.16 cm × 7.16 cm) and two plastic scintillators of the dimension (8 cm × 8 cm) (see Fig. 1). The plastic detectors are modeled as per the material specification of EJ212 [30], which is a special type of polyvinyl toluene (PVT) with a density of 1.023 g/cm^3. The composition is 8.47% Hydrogen and 91.53% Carbon. No reflective coatings or light absorbing materials was used in the model, following the final working design of the detector. The Si detectors are stacked parallel to each other, separated by air with a distance of 6 mm between each layer. The plastic scintillator detectors are placed upstream and downstream of the Si stack separated by air. The distance of the plastic detector from the Si stack is 4 mm on one side and 3 mm on the other side (Fig. 1). These are the closest possible distances between the last DSSSD and the plastic scintillator considering the restriction from the DSSSD frame and the space for the readout cables. The simulation has been carried out for two different standard thicknesses of Si layers, 300 μm and 1 mm respectively. The amount of light created by the plastic will depend upon the energy loss of the β particles. The thickness of the plastic should be chosen such that the light produced by the traversing β particles results in a signal above the noise level.

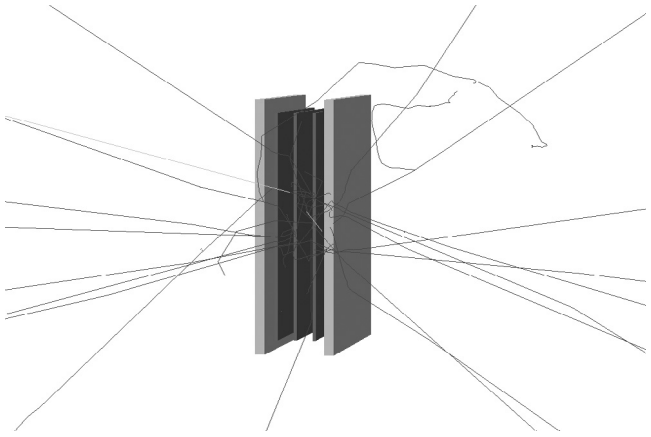

Fig. 1. The simulation consists of three DSSSD stacked in the center and two plastic scintillator detectors on both sides of the DSSSD detectors. The dark lines correspond to β particles and the gray lines are x-rays.

2.2. Physics process

Necessary physics interactions models were used in the simulation for cross-section calculation. The electromagnetic interactions were modeled by the Geant4 Standard Electromagnetic Package [31]. This package handles a number of interactions including multiple scattering, ionisation, Bremsstrahlung, positron annihilation, photoelectric effect, Compton and Rayleigh scattering and pair production [32]. The Package uses analytical methods to describe the interactions of energetic particles such as, the electrons, positrons, photons, and ions in the energy range of 1 keV–10 PeV. The package reproduces the NIST-ESTAR data set [33] for stopping power and range within 3σ uncertainty [32]. The NIST-ESTAR data set has an uncertainty in reproducing the stopping power of electrons between 1% and 10% for collision stopping power and in between 2% and 5% for radiative stopping power [34].

2.3. Simulation of the source

The depth distribution of the implanted fragments, in a typical DESPEC experiment will be centered at the middle layer of the DSSSD stack assembly. The depth profile is approximated by two different source profile distributions in the simulation. In the first case, the radioactive source is assumed to be uniformly distributed in the beam direction in each of the three layers of Si. The distribution perpendicular to the beam direction is assumed to be 2×1 cm^2 for all three layers of DSSSD. A second case is considered, where the source is assumed to be distributed uniformly only in the middle layer of the Si stack. In practice, the implanted ions are expected to be distributed in all three layers of the DSSSDs in varying quantity, centered around the middle layer. Hence, any real implantation distribution is somewhere in between these two limiting cases and the simulation results will thus give a systematic uncertainty to the actual response of the detector system. The angular distribution of the β-particles emitted from the implanted ions is an important factor of the simulated efficiency. The energy release of the heavy isotope at implantation will obstruct any

Please cite this article as: S. Saha, T. Arici, J. Gerl et al., On the β-detection efficiency of a combined Si and plastic stack detector for DESPEC, Nuclear Inst. and Methods in Physics Research, A (2020) 164196, https://doi.org/10.1016/j.nima.2020.164196.

β-decay measurement for ~1 μs after implantation of the fragment. Hence, in practice only β decay from the fully stopped fragments could be measured. Any correlations of the β-decay momentum direction distribution with respect to the implanted fragment momentum direction will be dependent upon the spin relaxation time scale of the implanted nucleus. If the spin relaxation time scale, which also depends on the nuclear temperature after fragmentation, is less than the time window between implantation of the fragment and detection of the subsequent β decay all directional correlation will be lost. Considering a waiting time larger than 1 μs after implantation for the detectable β decay events it could be argued that the β-decay momentum direction distribution with respect to the source positions is isotropic in most cases. As a result no corrections for boost of the fragment is applied in the simulation.

A simulated geometry and a few decay events are shown in Fig. 1. The source is assumed to be distributed in a rectangular area of 2 cm in the horizontal, X-direction, and 1 cm in vertical, Y direction, on the central Si layer. Simulations were carried out using the two different implantation profiles of the source distribution conditions in the Si layers as discussed above. The β-decay energy distribution can be user defined or the known β-decay energy distribution of any nuclei can be called from the Radioactive Decay data base of Geant4 [35]. The RadioactiveDecay data base follows the decay information from Evaluated Nuclear Structure Data File (ENSDF) (2013 version) [36]. The build in classes of Geant4 were used to construct the decay products and track the electrons after decay from the nuclei, considered here as the primary particles. The radioactive nuclei were created using the G4ParticleGun class. The standard user commands */gun/particle ion* and */gun/ion Z A* method was invoked via G4ParticleGunMessenger class to define the specific radioactive isotopes. The track of the radioactive nuclei was stopped invoking the *SetTrackStatus(fStopButAlive)* method on the primary track object of G4Track class. This has allowed the radioactive primary ions to decay at zero momentum. The beta decay of the daughter nuclei was prevented using *SetTrackStatus(fStopAndKill)* method. This process also stops deexcitation of the daughter via γ decay. This method helped simulation of only one β decay, whereas in general if the daughter nucleus is β unstable, it will follow the rest of the decay chain until a stable isotope is reached. In this way only the secondary particles such as electrons and anti-νs are tracked from the primary decay and the energy deposition from the interaction of the electrons with the detector material is measured. In an actual decay spectroscopy experiment β decay time stamps will be used to separately identify the decays in a decay chain.

The β decay from the parent to daughter and daughter to granddaughter nuclei will be separated by a time difference governed by the lifetime of the parent and daughter nuclei respectively. These lifetimes are significantly higher (of the order of ms to seconds) than the time resolution of the plastic detector (~100 ps). After implantation time stamp, the next decay events will be searched for within a few half life of the implanted isotope. The total transmitted ion rate is generally very low (<1 kHz) for the extremely rare isotopes that are planned to be studied in the DESPEC experiment [37]. The overall low rate of implantation will result into very low rate of accumulation of long lived β decaying isotopes to significantly affect the statistics by incorporating additional dead time to the detector and DAQ.

Nine nuclei from two different chain of isotopes, ^{206,207,208,209,210}Au and ^{128,130,132,134}In were simulated to calculate the efficiency response of the detector setup. These isotopes have different Q_β values and average energy of the β distribution, ranging from 5.7 (3) MeV to 14.8 (3) MeV and 2409 keV to 6937 keV, respectively.

A realistic β-decay energy distribution is calculated for ^{224}At and the uniform momentum distribution of emitted β particles were simulated. In Fig. 2, the calculated β-energy distribution for ^{224}At decay is shown. Due to the limitation of ENDSF data set, the application of the build-in decay data generator of Geant4 is limited. Hence, the Monte Carlo event generator DEGEN (Decay data Generator) is used for the generation of the β spectrum [38,39]. The statistical distribution of the β-decay peaks around 2 MeV and a significantly large probability of β decay is expected with energy ranging from 0–5 MeV.

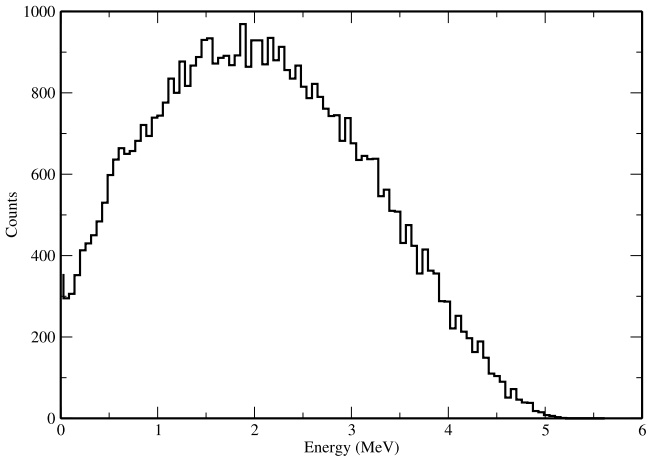

Fig. 2. Calculated beta energy distribution for ^{224}At with Q_β = 5.266(24) MeV [36].

3. Results and discussion

The simulated β-particles emitted from the decaying nuclei will have multiple scattering in between the DSSSDs and in the plastic. As the DSSSDs are electronically segmented into 128 X and 128 Y channels, with each strip size of 0.56 mm only, there will be many simulated events where several channel multiple hits will be recorded. The efficiency of the detector system is calculated after taking into account the multiple interaction probability of the electron with different strips of the same DSSSD and repeated counting by the same detector is avoided in the simulation. The electron momentum distribution, from the source position has been considered isotropic. The electrons will be energetically degraded and diffused while being transported through the Si detectors and air before reaching the plastic scintillator.

In Fig. 3 the hit pattern of electrons in the DSSSDs are shown, when 200 keV and 2 MeV electron sources are simulated with the same statistics. The plots in the top and bottom row represents the distribution profiles of 200 keV and 2 MeV electrons, while the first, second and third columns shows respectively the front, middle and back layers of a 1 mm thick DSSSD stack. The X and the Y axis represents the coordinates of the electron hit position in the detectors and the bin size represents the size of the DSSSD strips. The colors of the individual pixels correspond to the number of hits detected per pixel of the DSSSDs. The source is assumed to be implanted uniformly in depth of the central pixel of the middle layer of the DSSSD stack assembly. Due to possibility of multiple hits by the same electron, the number of hits recorded in the detectors are generally more than the number of primary electrons created. The range at which the statistics falls off significantly roughly represent the maximum range of electron from the source position after multiple random scattering within the detectors. In both cases, (200 keV and 2 MeV) the pixel where the source is implanted counted the most statistics and a gradual depletion of counts with increasing distance from the central pixel is observed. The overall number of hits detected in the middle DSSSD is much larger for electrons with 200 keV energy (Fig. 3b) compared to 2 MeV (Fig. 3e) energy. On the other hand, hit counts increases in the peripheral DSSSDs for 2 MeV compared to 200 keV electrons. This can be observed from the counts scale in the color-coded plot. This difference is observed due to the expected range of electron in the DSSSD is larger at higher energies. On the other hand, the front and back DSSSDs see much lower counts for 200 keV electrons (Fig. 3a and c) compared to 2 MeV (Fig. 3d and f). The distribution profile is much narrower for the low energy electrons than at higher energies. The reason for wider distribution at higher energies can be explained by the increase of the number of multiple scattering of the electrons interacting with the neighboring DSSSDs.

Please cite this article as: S. Saha, T. Arici, J. Gerl et al., On the β-detection efficiency of a combined Si and plastic stack detector for DESPEC, Nuclear Inst. and Methods in Physics Research, A (2020) 164196, https://doi.org/10.1016/j.nima.2020.164196.

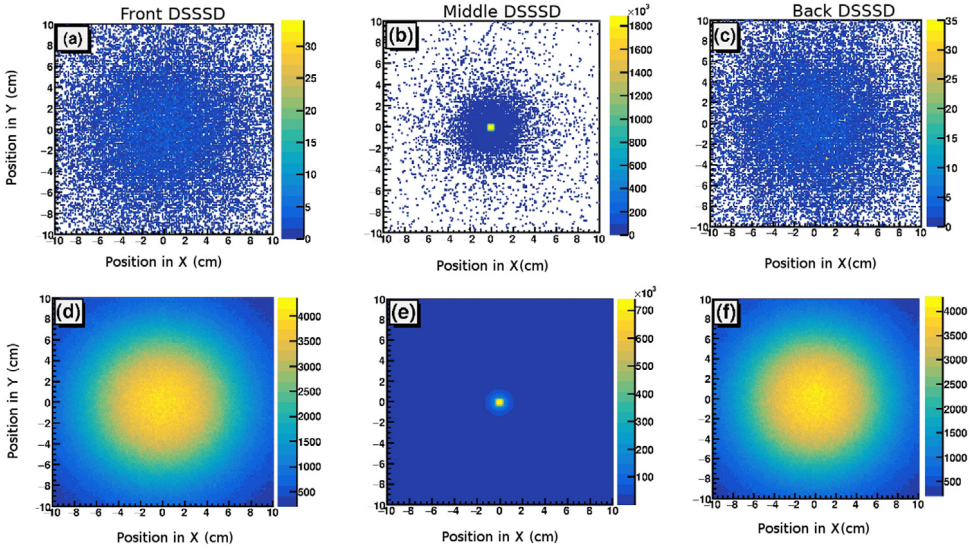

Fig. 3. The hit pattern of electrons in the three DSSSDs when the source is uniformly distributed in the central pixel of the middle layer only. Panel (a)–(c) shows the hit pattern with 200 keV electron source and panel (d)–(f) shows the same for 2 MeV electrons source. The first, second and the third columns represents respectively, the front, middle and back layer of the DSSSD stack.

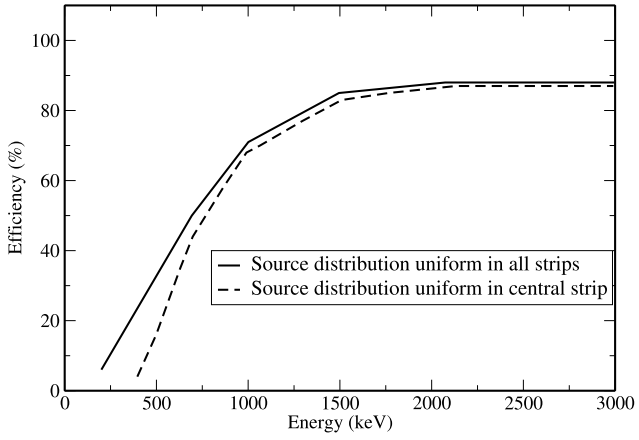

Fig. 4. Efficiency of plastic for 300 μm thick Si layers.

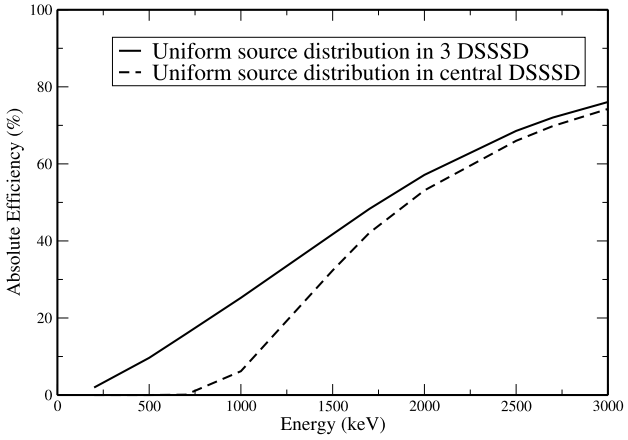

Fig. 5. Efficiency of plastic scintillators for 1 mm thick Si layers.

The energy dependence of the efficiency of the detector system is calculated in steps with mono-energetic and isotropic β sources of 200 keV to 3 MeV. The efficiency is defined as the ratio of the electrons detected above the threshold vs. the number of β-particles simulated in the source. Combined efficiency of the two plastic detectors is calculated for a thin (300 μm) and thick (1 mm) DSSSD assembly. Fig. 4, shows the absolute efficiency of the plastic detector simulated with 300 μm Si layers in the minimum possible distance configuration. The dashed line represents the efficiency obtained when the source is uniformly distributed in the center layer of the Si (along the Z direction, *i.e.* thickness of the Si detector). The solid line represents the case when the source is uniformly distributed in all three layers of the Si. The actual distribution (if assumed to be a Gaussian) will be centered at the middle layer of Si and distributed in all 3 DSSSD layers. These two curves roughly represent the maximum and the minimum β efficiency of the plastic detector for these two extremes of the source implantation distribution.

The drop in efficiency of the plastic detector at electron energy less than 1.5 MeV is consistent with the expected absorption of electrons in the DSSSD at low energy. A considerable number of electrons emitted from the source implanted in the middle layer of the DSSSD stack does not reach the plastic detectors after losing energy in the Si and air layers. The number of electrons detected in plastic detector is less for source implanted in the central DSSSD compared to all DSSSDs, because in the former case the electrons travel through thicker layers Si and air. Since at higher energy more electrons will reach to the plastic detectors from the central DSSSD, the difference in the efficiency in these two cases decreases with increase in energy of the electron. Similarly, simulation study with 1 mm thick Si layers is shown in Fig. 5. The efficiency of the plastic detector remains below 80% up to 3 MeV with an increasing slope. This represents a sharp drop in overall efficiency of the plastic detector when a thicker Si stack is used, as a result of increased stopping of low energy electrons.

Further simulations have been carried out to observe the dependencies of efficiency on the distance between Si and plastic detectors. Due to operational reasons the distances between the DSSSDs could not be reduced any further. The corresponding plot for minimum distance configuration and 10 mm distance between outer Si layer and the plastic in both sides of the stack is shown in Fig. 6. This plot indicates a minor improvement in the efficiency from 71% at 10 cm distance to 74% at minimum distance for 3 MeV β particle when the detectors are brought closer. However, for low energy electrons no increase in efficiency is observed. For a distance variation from minimum distance configuration to 10 mm distance of the plastic detector only marginal

Please cite this article as: S. Saha, T. Arici, J. Gerl et al., On the β-detection efficiency of a combined Si and plastic stack detector for DESPEC, Nuclear Inst. and Methods in Physics Research, A (2020) 164196, https://doi.org/10.1016/j.nima.2020.164196.

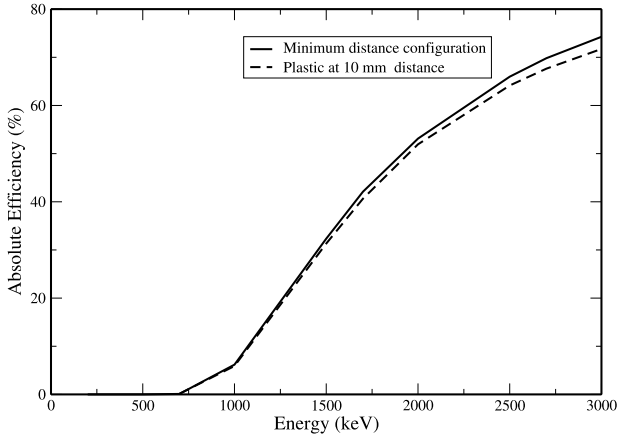

Fig. 6. Plot of efficiency for different distances between plastic and outer Si layer. Source position uniformly distributed at the central Si layer only.

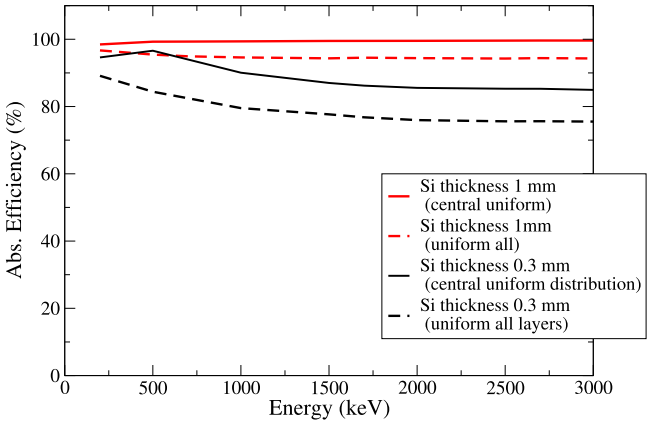

Fig. 7. Plot of the efficiency of DSSSD as a function of energy of the emitted β particles for 0.3 mm and 1 mm thickness. (For interpretation of the references to color in this figure legend, the reader is referred to the web version of this article.)

improvement in efficiency is noticed. Each of the 128 strips in x direction, of the AIDA DSSSD, is considered to have a threshold of 100 keV. Due to the multiple scattering of electrons, energy sharing among different strips, is likely resulting in multi-hit events, provided the energy deposited in the respective strips, is higher than the threshold. Hence, the strip-wise threshold is needed to be considered in the simulation. In Fig. 7, the efficiency of the electrons for different energies above the threshold has been plotted for 0.3 mm (black) and 1 mm (red) thick DSSSD detectors in minimum distance configuration of the AIDA assembly. The solid lines corresponding to the fragment implantation at the central layer (leading to higher detection efficiency) while the dashed line corresponds to uniform fragment implantation in all layers of the Si stacks respectively. The efficiency of the 1 mm Si detector remains higher than that of the 0.3 mm at all energies in both source configurations.

It should be noted that for typical decay experiments the energy distribution of the β particles falls off rapidly above 2 MeV as shown in Fig. 2. On the other hand, the plastic detector efficiency increases up to 1.5 MeV and becomes almost flat at higher energies as shown in Fig. 4. For this reason, a straight forward estimation of the combined efficiency is difficult for a realistic β-decay case and requires detailed simulation of the source energy distribution for each isotope of interest. As a typical example, the β-decay energy distribution of ^{224}At is approximated with a polynomial and a random distribution of β-decay events following the energy distribution is generated. The implanted source distribution profile is again considered to be uniformly distributed in all Si layers and in the middle layer only. For this isotope the total efficiency of the two plastic detectors together for an assumed middle layer distribution is 75.5% and for a uniform distribution in all layers it is $\sim$ 78.0%. For a thick (1 mm) DSSSD stack, simulation of uniformly implanted ^{224}At β-decay distribution in the middle layer of the Si only provides 45.8% efficiency, while the same for all layers of Si provides 52.8% efficiency in the plastic detector. The detection efficiency for the 1 mm thick DSSSD detectors for the ^{224}At β decay, with fragments uniformly distributed in the middle layer of the Si is 98.7% while the same for uniform distribution in all layers of the Si is 93.9%. The efficiency for 0.3 mm thick DSSSDs is respectively 86.5% and 76.3%, for uniform central distribution and uniform in all Si distribution configurations. The combined efficiency of plastic and AIDA Si of the calculated ^{224}At decay will be between 45%–48% for 1 mm and between 60%–65% for 0.3 mm Si respectively.

In Fig. 8, the combined efficiency of the DSSSDs and plastic detectors for β decay of ^{206,207,208,209,210}Au and ^{128,130,132,134}In isotopes as a function of the average electron energy are plotted. The calculated efficiencies of the β-decaying nuclei are considered to be the average of the two different source profile distributions considered in the simulation, while the difference in the efficiency for these two distributions are the systematic uncertainties. For the detector setup with 1 mm thick DSSSD, the uncertainty increases with increase in the average energy of the β-decay distribution while it remains almost same for 300 μm DSSSD. It has also been observed, that the systematic uncertainty in efficiency is larger for 300 μm DSSSD as compared to the 1 mm DSSSD stack. This is due to the fact that the electron momentum distribution becomes more diffused and isotropic when number of multiple scattering is increased. Hence, as shown in Fig. 6, when the distance between source position and detector increases, the efficiency is reduced more at higher energies. For the uniform source distribution in all DSSSD configuration the effective distance between the source position and detector is increased than the uniform central distribution configuration. The thin DSSSD stack having much less screening effect than the thick stack, leads to more events being detected in the furthest plastic detector. This increases the average efficiency and the systematic uncertainty for thin DSSSD stack relative to the thick DSSSD at lower energies. At higher energies of β distribution for the thick DSSSD become more opaque to the electrons and the efficiencies of both detector setups become comparable. The absolute efficiency of the setup for 1 mm thick DSSSD increases smoothly from ~50% for ^{207}Au to ~80% for ^{134}Sn nuclei. Whereas, the efficiency remains almost same for all these isotopes when the DSSSDs thickness is reduced to 300 μm. In Table 1, the calculated efficiency with there respective systematic errors for each isotopes are shown, along with their Q_β values and average energy of β for the setup comprising of 1 mm and 300 μm DSSSDs respectively.

The efficiency will change for different possible shapes of the implanted ions. The simulations were carried out assuming a rectangular distribution of 2 × 1 cm^2. The shape of the implanted fragment distribution was varied to calculate the resulting deviation in the efficiency of the detector. The source distribution was assumed to be uniform in depth over all three 300 μm thick DSSSD detectors for this simulation. The total β efficiency of the detector for a few different shapes, namely a square, a uniform circular and a Gaussian circular distribution of dimensions respectively, 1 × 1 cm^2, 1 cm diameter and 1 cm diameter at the FWHM are calculated along with the rectangular type distribution mentioned above. A 1 MeV and a 5 MeV electron source energy was considered for this calculation. The resulting variation in efficiencies of the square, uniform circular and Gaussian circular distributions from the square shaped distribution are less than 0.2% at 1 MeV and 0.7% at 5 MeV. It can be concluded, that for a small central implantation distribution the shape of the distribution does not play a significant role in the overall efficiency of the detector.

The primary implantation fragment with A/Q ratio corresponding to the central Bρ value of the separator will be centered (in the X-Y

Please cite this article as: S. Saha, T. Arici, J. Gerl et al., On the β-detection efficiency of a combined Si and plastic stack detector for DESPEC, Nuclear Inst. and Methods in Physics Research, A (2020) 164196, https://doi.org/10.1016/j.nima.2020.164196.

Table 1
Simulated absolute efficiencies for β-decay measurement of implanted ^{206,207,208,209,210}Au and ^{128,130,132,134}In isotopes for the setup consist of 1 mm and 300 μm thick DSSSD stack have been plotted along with their respective Q_β and average β spectrum energy (β_{avg}). The quoted error in the efficiency is the systematic uncertainty in efficiency from two different source profile distribution as mentioned in the text.

Name	Q_β (keV)	β_{avg} (keV)	Abs. Efficiency (1 mm DSSSD)	Abs. Efficiency (300 μm DSSSD)
^{207}Au	5.7×10^3(3)	2409	53.96 (4)	63 (4)
^{209}Au	6.1×10^3(3)	2644	57.4 (3)	64 (4)
^{206}Au	6.7×10^3(3)	2884	60.8 (3)	64 (4)
^{208}Au	7.2×10^3(3)	3090	63.1 (6)	65 (4)
^{210}Au	7.7×10^3(4)	3328	65.7 (10)	65 (4)
^{128}In	9.22×10^3(15)	2814	59.3 (1)	64 (4)
^{130}In	1.025×10^4(4)	3072	62.6 (5)	65 (4)
^{132}In	1.414×10^4(6)	3592	68.2 (11)	66 (4)
^{134}In	1.48×10^4(3)	6937	80.3 (22)	65 (5)

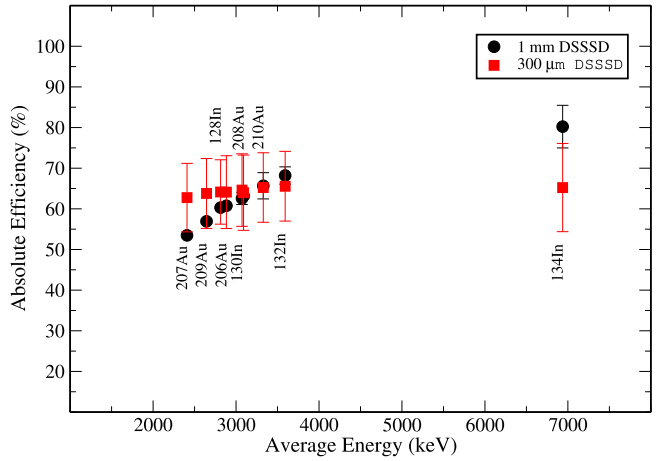

Fig. 8. Absolute efficiency of ^{206,207,208,209,210}Au and ^{128,130,132,134}In isotopes are plotted as a function of average energy of their β-decay distribution. The efficiency of 1 mm and 300 μm thick DSSSD is shown in filled circles and open squares, respectively. The name of the isotope is shown next to the data point representing the calculated efficiency.

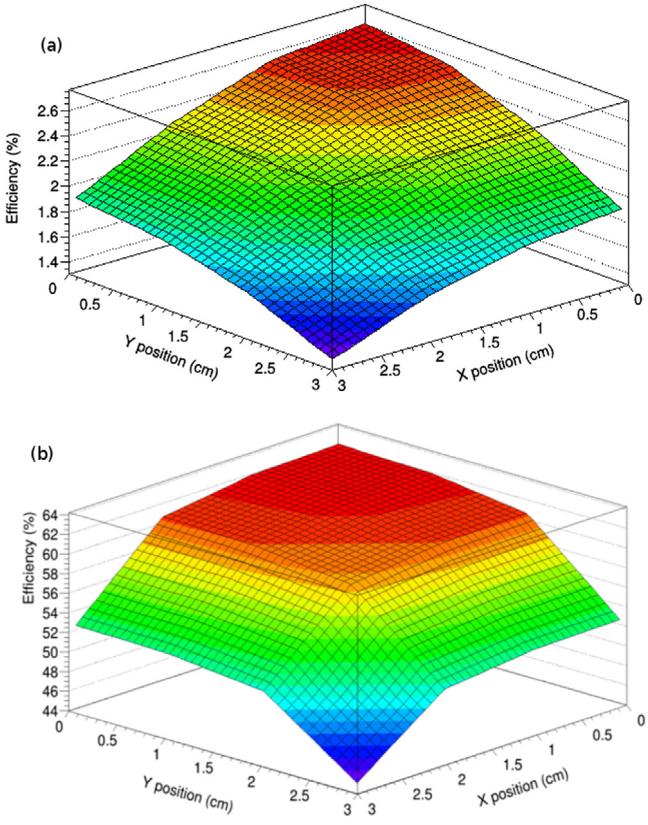

Fig. 9. The combined total efficiency of the DSSSDs and plastic detectors for a simulated 1 MeV electron source is plotted as a function of source implantation position on 300 μm DSSSD detectors. The panel (a) shows the efficiency plot for various source positions in the front DSSSD and panel (b) shows the same for source positions in the central DSSSD.

plane) with respect to the DSSSD detector. However, fragments with non-central Bρ will be focused at other positions of the DSSSD detector. The position distribution of the fragments will be dependent upon the respective settings of the fragment separator. The dependence of efficiency on the XY position of the source distribution is estimated by simulating a 1 MeV electron source placed at various source positions in the first quadrant of the DSSSD detector. A symmetric efficiency distribution in all four quadrants with respect to the center of the DSSSD is expected. The efficiency is simulated at 16 grid points separated by 1 cm from the origin up to 3 cm at the positive X and positive Y directions. The plots representing the calculated efficiency for the front and central DSSSDs are shown as Fig. 9(a) and (b) respectively. The total efficiency of the detector is much less for implantation in the front and back DSSSD compared to the implantation in the middle DSSSD. Also, efficiency reduces by a small 0.4% when the source position is shifted by 1 cm in the X or Y direction. However, the efficiency reduces by 2.5% and 16% of the value at origin when the source is shifted by further 2 cm and 3 cm, respectively. It is also observed that the rate of change in efficiency along the diagonal is comparatively less than that along the axes. In this simulation the thickness of the DSSSD is considered to be 300 μm. Due to low stopping power for individual DSSSD's in this case, more electrons from the central DSSSD is expected to get scattered and detected by the plastic detectors on both side of the stack compared to the electrons sourced from the front or back DSSSDs. At this energy around 92% contribution to the total efficiency of the detector comes from the implantation of fragments in the central DSSSD alone.

The total efficiency of the setup will depend upon the threshold of the detectors. It can be seen in Figs. 4 and 5 that the efficiency of the plastic detector below an energy of 150 keV is practically negligible for both 1 mm and 300 μm DSSSD stacks. This requires the threshold of the plastic detector to be at least 150 keV without loss of efficiency. However, the higher DSSSD threshold significantly reduces the total efficiency. Due to the high stopping power of DSSSD, only higher energy electrons will be able to scatter through the DSSSDs and reach the plastic detector. This makes the total efficiency of the detector less affected by the plastic threshold compared to the DSSSD threshold. The DSSSD threshold becomes even more important to the total efficiency, due to the higher efficiency of the detectors for low energy electrons (Fig. 7). On the other hand, the loss of electron energy in the plastic detector is negligible. Experimentally, the threshold for the plastic scintillator will come from the number of light photons generated from a valid event in the scintillator and the level of background noise

Please cite this article as: S. Saha, T. Arici, J. Gerl et al., On the β-detection efficiency of a combined Si and plastic stack detector for DESPEC, Nuclear Inst. and Methods in Physics Research, A (2020) 164196, https://doi.org/10.1016/j.nima.2020.164196.

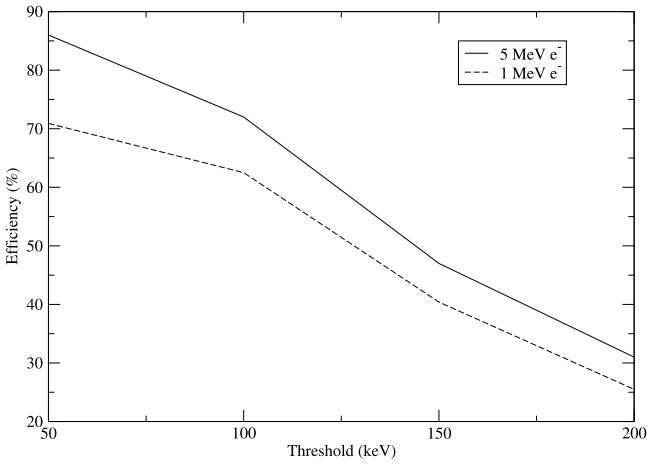

Fig. 10. The combined efficiency of the setup with 300 μm DSSSD stack with 1 MeV and 5 MeV point e^- source embedded in the middle of the central DSSSD stack is plotted for various threshold of the DSSSD ranging from 50 keV to 200 keV.

photons detected with the signal. For DSSSD detectors the number of thermal electron hole (e-h) pairs created in the Si detector vs the number of e-h pairs created from interaction of β particle will define the threshold. For AIDA setup the conservative estimate of threshold of the DSSSD detector is 100 keV.

The total efficiency of the DSSSD and plastic detectors are studied while varying the thresholds of the DSSSD detectors and the plastic detectors independently from 50 keV to 200 keV with a 5 MeV point electron source placed at the center of the middle DSSSD. The combined efficiency decreases marginally by less than 1% only when the threshold of the plastic detector increased from 50 keV to 200 keV. This trend is observed for both setups with 300 μm and 1 mm thick DSSSD. However, when the threshold of the plastic detector is kept constant at 100 keV and the DSSSD threshold is increased from 50 keV to 200 keV the change in efficiency is very different for 1 mm and 300 μm Si stack. For the 1 mm thick DSSSD the efficiency is reduced by a nominal 2%, while for the 300 μm thick DSSSD stack it is reduced by more than 50%. The large drop in efficiency at higher energy threshold is understood from the relatively small amount of energy deposition in the thin Si detectors compared to the thick detector stack. The combined efficiency is plotted in Fig. 10 with respect to the threshold of the DSSSDs for 300 μm DSSSD stack for 1 MeV and 5 MeV electron beam. Although, the overall efficiency of the detectors for the 1 MeV electron energy is less than that of the 5 MeV, the fall in efficiency shows similar trend for both the results. The result also suggests that for a broad β decay energy spectrum (Fig. 2), statistics will be primarily reduced by the same amount at various energies with the increase in detector threshold.

4. Conclusions

The simulation demonstrates the requirement for bringing the β-plastic detector the closest possible to the Si layers and reducing the thickness of the Si layers to improve the β-detection efficiency in the plastic detectors. The improvement in efficiency with further closely pack geometry is only marginal and relevant for high energy electrons only. The combined efficiency of the detector system improves from the range of 45%–48% for 1 mm to the range of 60%–65% for 0.3 mm Si respectively. However, such wider difference is observed when the average energy β decay distribution is lower than 2500 keV. Absolute efficiencies were calculated from the β-decay distribution of ^{206,207,208,209,210}Au and ^{128,130,132,134}In isotopes. These nuclei have Q_β values and average β-decay energies ranging from 5.7 MeV to 14.8 MeV and 2.4 MeV to 6.9 MeV respectively. The absolute efficiency of the setup increases smoothly when 1 mm thick DSSSD stack was used. However, the distribution of the efficiency as a function of average energy shows almost flat variation when 300 μm Si is used in this energy range. It can be concluded from this simulation that for experiments where the expected average β-decay energy is lower than 2500 keV the thin DSSSD performs better while above 3500 keV the thick DSSSD gives better efficiency. However, from ~2500 keV to 3500 keV their performance are more or less similar. Since a thinner stack of Si layers will effectively reduce the stopping power for the radioactive fragments, the fragment energy will needed to be suitably reduced before implantation. The effect of slowing down of fragments before implantation on the rate of implanted fragments, need to be investigated further. In this simulation, the efficiency is calculated for a 2×1 cm^2 centered distribution of the fragments, which will differ from an off-centered distribution or a different distribution profile. Combining the simulation result from fragment distribution profile would be necessary to further improve the accuracy of the efficiency expected in a typical decay spectroscopy experiment.

CRediT authorship contribution statement

S. Saha: Conceptualization, Software, Formal analysis, Writing - original draft, Writing - review & editing. **T. Arici:** Writing - review & editing. **J. Gerl:** Supervision, Writing - review & editing, Funding acquisition, Project administration. **M. Górska:** Supervision, Writing - review & editing, Funding acquisition, Project administration. **N. Pietralla:** Funding acquisition, Writing - review & editing. **T. Davinson:** Writing - review & editing. **A.I. Morales:** Writing - review & editing. **Zs. Podolyák:** Writing - review & editing.

Declaration of competing interest

The authors declare that they have no known competing financial interests or personal relationships that could have appeared to influence the work reported in this paper.

Acknowledgments

This work was supported by the BMBF under grant no. 05P19RDFN1 and by the cooperation between TU Darmstadt and GSI. Zs. Podolyák was supported in part by the ExtreMe Matter Institute EMMI at the GSI Helmholtzzentrum für Schwerionenforschung, Darmstadt.

References

[1] A.J. Mitchell, et al., The X-Array and SATURN: A new decay-spectroscopy station for CARIBU, Nucl. Instrum. Methods A 763 (2014) 232–239.
[2] K. Pourtangestani, R. Machrafi, Optimization of plastic scintillator thicknesses for online beta/gamma detection, EPJ Web Conf. 24 (2012) 07010.
[3] L. Miramonti, A plastic scintillator detector for beta particles, Radiat. Meas. 35 (2002) 347.
[4] F.K. Wohn, J.R. Clifford, G.H. Carlson, W.L. Talbert, A plastic scintillation detector for beta-ray spectrum measurements, Nucl. Instrum. Methods 101 (1972) 343.
[5] R. Kumar, et al., Testing of a DSSSD detector for the stopped RISING project, Nucl. Instrum. Methods A 598 (2009) 754.
[6] https://fair-center.eu/user/experiments/nustar/experiments/hispecdespec/despec.html.
[7] B. Rubio, Decay spectroscopy (despec) at the new fair-nustar facility, Internat. J. Modern Phys. E 15 (2006) 1979.
[8] https://fair-center.eu/for-users/experiments/nustar.html.
[9] B. Rubio, T. Nilsson, NUSTAR, Nucl. Phys. News 16 (2006) 9.
[10] https://www.gsi.de/start/aktuelles.html.
[11] J. Eschke, International facility for antiproton and Ion research (FAIR) at GSI, Darmstadt, J. Phys. G: Nucl. Part. Phys. 31 (2005) S967.
[12] R. Krucken, The NuSTAR facility at FAIR, J. Phys. G 31 (2005) S1807.
[13] F. Browne, et al., Lifetime measurements of the first 2^+ states in ^{104,106}Zr: Evolution of ground-state deformations, Phys. Lett. B 750 (2015) 448.
[14] S. Nishimura, Beta-gamma spectroscopy at RIBF, Prog. Theor. Exp. Phys. 2012 (2012) 03C006.

Please cite this article as: S. Saha, T. Arici, J. Gerl et al., On the β-detection efficiency of a combined Si and plastic stack detector for DESPEC, Nuclear Inst. and Methods in Physics Research, A (2020) 164196, https://doi.org/10.1016/j.nima.2020.164196.

[15] A.I. Morales, et al., Is seniority a partial dynamic symmetry in the first $\nu g_{9/2}$ shell?, Phys. Lett. B 781 (2018) 706.
[16] Technical Report for the Design, Construction and Commissioning of the Advanced Implantation Detector Array (AIDA), https://edms.cern.ch/document/1865809/1.
[17] AIDA web page, https://www2.ph.ed.ac.uk/td/AIDA/, and, C. Griffin, Ph.D. thesis, University of Edinburgh (2019), to be published.
[18] HISPEC/DESPEC TDR, to be published, and, Zs. Podolyák, From RISING to HISPEC/DESPEC, Nucl. Instrum. Meth. B 266 (2008) 4589.
[19] C.B. Hinke, et al., Superallowed Gamow-Teller decay of the doubly magic nucleus 100Sn, Nature 486 (2012) 341–345.
[20] S.J. Steer, et al., Isomeric states observed in heavy neutron-rich nuclei populated in the fragmentation of a ^{208}Pb beam, Phys. Rev. C 84 (2011) 044313.
[21] O. Roberts, et al., A LaBr3: Ce fast-timing array for DESPEC at FAIR, Nucl. Instrum. Methods Phys. Res. A 748 (2014) 91.
[22] Technical Report for the Design, Construction and Commissioning of the Fast Timing Array (FATIMA), https://edms.cern.ch/document/1865981/1.
[23] Zs. Podolyák, Studies of exotic nuclei with advanced radiation detectors, Radiat. Phys. Chem. 95 (2014) 14.
[24] S. Lalkovski, et al., The UK NuStAR PROJECT, Acta Phys. Polon. B 47 (2016) 637.
[25] M. Rudigier, et al., Fast timing measurement using an LaBr3(Ce) scintillator detector array coupled with gammasphere, Acta Phys. Pol. B 48 (2017) 351.
[26] H. Geissel, et al., The Super-FRS project at GSI, Nucl. Instrum. Methods Phys. Res. B 204 (2003) 71.
[27] H. Geissel, et al., The GSI projectile fragment separator (FRS): a versatile magnetic system for relativistic heavy ions, Nucl. Instrum. Methods B 70 (1992) 286–297.
[28] S. Agostinelli, et al., GEANT4: a simulation toolkit, Nucl. Instrum. Methods A 506 (2003) 250.
[29] S. Saha, et al., Geant4 simulation study of Indian National Gamma Array at TIFR, J. Instrum. 11 (2016) P03030.
[30] https://eljentechnology.com/products/plastic-scintillators/ej-200-ej-204-ej-208-ej-212.
[31] V.N. Ivanchenko, M. Maire, L. Urban, Geant4 standard electromagnetic package for HEP applications, in: Proc. Conf. Rec. 2004 IEEE. Nuclear Science Symp. Rome, Italy. Paper code: N33-179.
[32] K. Amako, et al., Comparison of Geant4 electromagnetic physics models against the NIST reference data, IEEE Trans. Nucl. Sci. 52 (4) (2005) 910.
[33] M.J. Berger, J.S. Coursey, D.S. Zucker, ESTAR, PSTAR, and ASTAR: Computer Programs for Calculating Stopping-Power and Range Tables for Electrons, Protons, and Helium Ions (Version 1.2.2), National Institute of Standards and Technology, Gaithersburg, MD, 2000.
[34] Stopping Powers for Electrons and Positrons, ICRU Rep. 37, International Commission on Radiation Units and Measurements, Bethesda, MD, 1984.
[35] S. Hauf, et al., Validation of geant4-based radioactive decay simulation, IEEE Trans. Nucl. Sci. 60 (4) (2013) 2984.
[36] National Nuclear Data Center, Evaluated Nuclear Structure Data Files. http://www.nndc.bnl.gov/ensdf.
[37] Zs. Podolyák, et al., Heavy nuclei studied in projectile fragmentation, Nuclear Phys. A 722 (2003) C273.
[38] A. Algora, E. Nácher, private communication.
[39] D. Jordan, et al., An event generator for simulations of complex β-decay experiments, Nucl. Instrum. Methods A 828 (2016) 52–57.

Please cite this article as: S. Saha, T. Arici, J. Gerl et al., On the β-detection efficiency of a combined Si and plastic stack detector for DESPEC, Nuclear Inst. and Methods in Physics Research, A (2020) 164196, https://doi.org/10.1016/j.nima.2020.164196.